Supporting Information:

Boosting the thermoelectric performance of (Na, K) co-doped polycrystalline SnSe by synergistic tailoring of the band structure and atomic-scale defect phonon scattering

Zhen-Hua Ge[#, †], Dongsheng Song[§, †], Xiaoyu Chong[#, ₸, †] Fengshan Zheng[‡, *], Lei Jin[‡], Xin Qian[ǁ], Lei Zheng[ǁ], Rafal E. Dunin-Borkowski[‡], Peng Qin[#], Jing Feng[#, *], Li-Dong Zhao[ǁ, *]

#Faculty of Materials Science and Engineering, Kunming University of Science and Technology, Kunming 650093, China.

§National Center for Electron Microscopy in Beijing, Key Laboratory of Advanced Materials (MOE), School of Materials Science and Engineering, Tsinghua University, Beijing 100084, China.

‡Ernst Ruska-Centre for Microscopy and Spectroscopy with Electrons and Peter Grünberg Institute, Forschungszentrum Jülich, 52425 Jülich, Germany.

ǁSchool of Materials Science and Engineering, Beihang University, Beijing 100191, China.

₸Department of Materials Science and Engineering, The Pennsylvania State University, University Park, PA 16802, USA.

†These authors contribute equally to this work.

*Corresponding authors: f.zheng@fz-juelich.de, jingfeng@kmust.edu.cn, zhaolidong@buaa.edu.cn.

I. Sample Synthesis

High purity Sn (99.99%, powder), Se (99.99%, Powder), Na (99.9%, Chunks), and K (99.9%, Chunks) were weighed in a glove box in an Ar atmosphere. The Na, K and dual-doped SnSe powders were prepared by mechanical alloying at 425 rpm for 5 h, according to the composition $Na_xK_ySn_{1-x-y}Se$, (x = 0, 0.005, 0.01, y = 0, 0.005, 0.01), in a mixed atmosphere of Ar (95%) and H_2 (5%) using a planetary ball mill (QM-3SP4, Nanjing University, China). Stainless steel vessels and balls were used, with a weight ratio of ball to powder of 20:1. The ball-milled powders were sintered at 773 K for 5 min in a Φ20 mm graphite mold under an axial pressure of 50 MPa in vacuum using a spark plasma sintering (SPS) system (SPS-211Lx, Japan).

Table S1 Measured density and relative density

Sample	**Measured density (g/cm^3)**			**Average density (g/cm^3)**	**Relative density (%)**
	1	2	3		
undoped	5.82	5.89	5.93	5.88	94.8
1% Na	5.79	5.83	5.78	5.80	93.5
0.5%Na+0.5%K	5.70	5.69	5.73	5.71	92.0

Transport property measurements

The sintered specimens were disk-shaped with dimensions of Φ20 mm × 8 mm. After cutting and grinding, two samples were obtained. One sample was stripe-like with dimensions of ~ 3 mm × 4 mm × 13 mm for electrical conductivity/Seebeck coefficient measurements, while the other was disk-like with dimensions of ~ Φ 6 mm × 1 mm for thermal conductivity measurements. Thermoelectric transport properties were evaluated along a sample section perpendicular to the SPS pressing direction. The morphologies of fractographs were investigated by field emission scanning electron microscopy (FESEM, Zeiss Merlin, Germany). TEM samples were prepared by focused ion beam (FIB) milling using an *in situ* lift-out technique. TEM investigations were conducted using FEI

Tecnai F20 and T20 microscopes. The Seebeck coefficient and electrical conductivity were measured between 300 and 773 K in a He atmosphere using a Seebeck coefficient/electric resistance measuring system (ZEM-3, Ulvac-Riko, Japan). The thermal conductivity κ was calculated from the relationship $\kappa = DC_p d$, with the density d measured by the Archimedes method and the thermal diffusivity D measured by a laser flash method (NETZSCH Laser Flash Apparatus LFA 457, Germany). The specific heat C_p was taken from Ref. 1. The combined uncertainty of the experimental determination of *ZT* was ~ 15-20%, originating from the measurement of electrical conductivity, Seebeck coefficient, thermal diffusion coefficient, heat capacity and sample density. The Hall coefficient (R_H) was measured at 323 K using a physical property measurement system (PPMS-9T, Quantum Design Inc., USA) with a magnetic field of 2 T and an electrical current of 30 mA. The carrier concentration (n) was calculated from the expression $n=1/eR_H$, where e is the electronic charge. The carrier mobility (μ) was calculated from the expression $\mu=R_H/\rho$.

II. X-ray diffraction and FESEM characterization

The crystallographic phase structure was analyzed by X-ray diffraction (XRD, Cu-K_α, Riguku, Japan). Both in-plane and out-of-plane XRD for the polycrystalline SnSe samples were measured, as shown in Figure S1. Because the samples were fabricated by mechanical alloying and spark plasma sintering, results in a polycrystalline sample with small grain size, no significant crystal orientation observed. The little stronger intensity of (400) indicates slight texture produced, the SEM images in Figure S2 shows these textures, These results are agreement with the XRD analysis. The texture microstructures will affect the electrical and thermal transport properties, thus we investigated the thermoelectric transport properties along the two directions that are parallel and perpendicular to the SPS pressing direction (Figure S3). The result shows that the sample in the direction perpendicular to the pressing direction has the higher electrical conductivity, the lower Seebeck coefficient, the higher thermal conductivity and the higher *ZT* value. Therefore, the thermoelectric transport properties for all the samples in this study were investigated along the direction that is perpendicular to the SPS pressing direction.

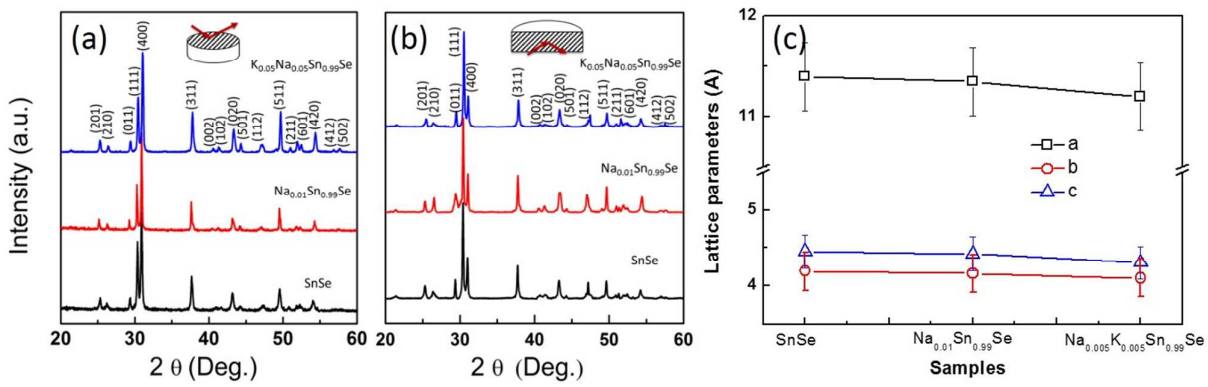

Figure S1 (a) XRD patterns along in-plane and (b) out-of-plane, and (c) lattice parameters of undoped, 1% Na-doped and 0.5% Na + 0.5% K co-doped polycrystalline SnSe.

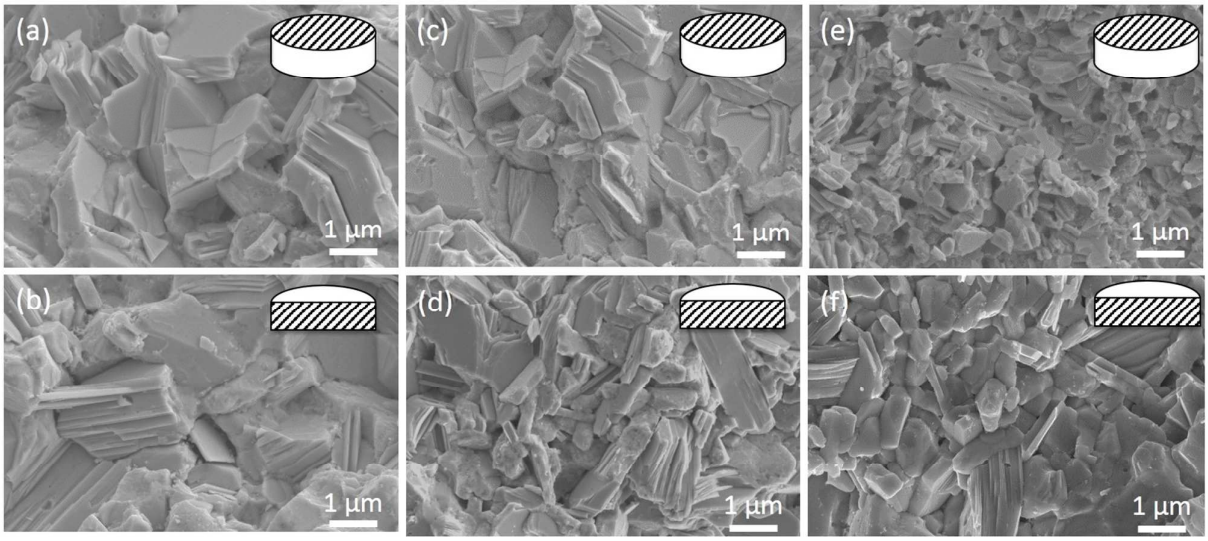

Figure S2 FESEM images of (a-b) undoped, (c-d) 1% Na sample and (e-f) 0.5% Na+0.5% K sample.

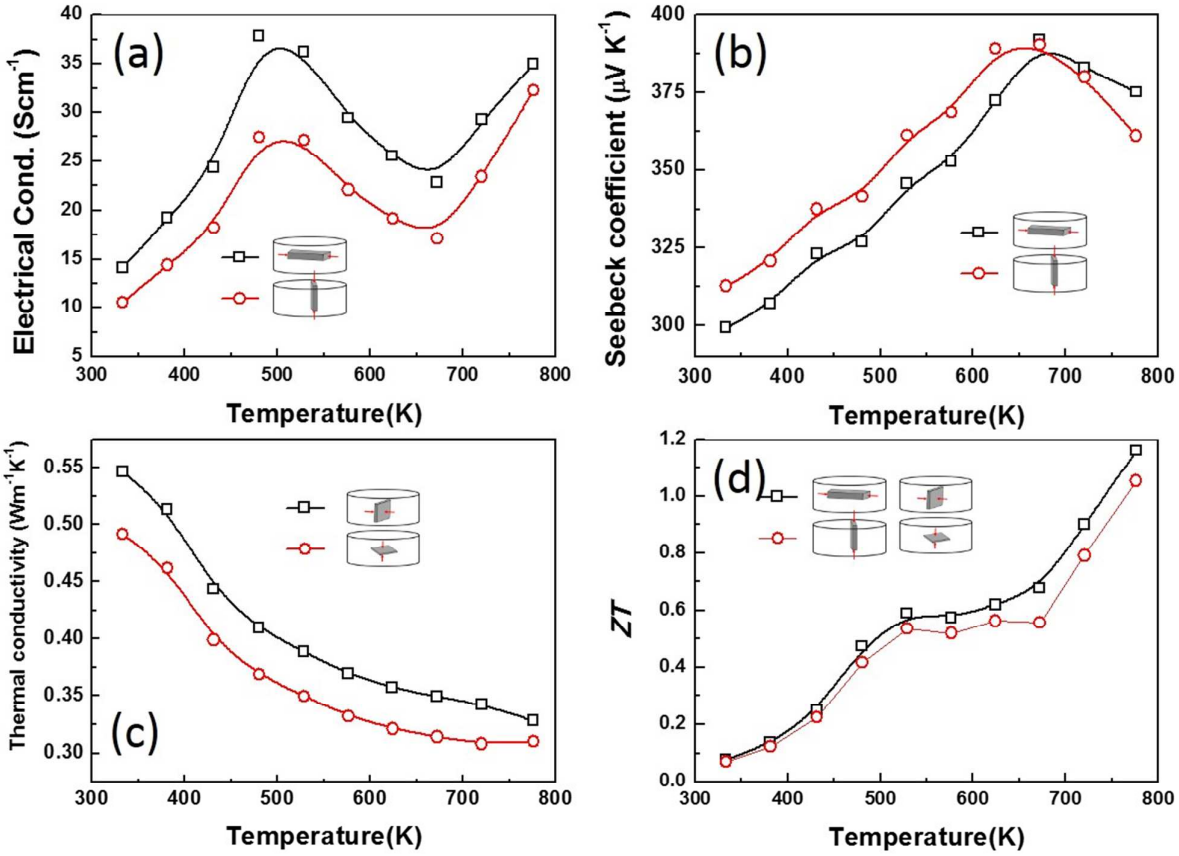

Figure S3 Temperature dependence of (a) electrical conductivity, (b) Seebeck coefficient, (c) thermal conductivity and (d) *ZT* values for 0.5%Na+0.5%K sample in the directions both perpendicular and parallel to the SPS pressing direction.

III. Density functional theory calculations

Density functional theory (DFT) calculations were carried out using Ultrasoft pseudopotentials, as implemented in the Cambridge sequential total energy package (CASTEP) code[2,3], for structural relaxation. The exchange-correlation functional was defined using a generalized gradient approximation (GGA) of the Perdew-Burke-Ernzerhof (PBE) functional. The Heyd-Scuseria-Ernzerh hybrid functional (HSE06)[4,5], which adopts a screened Coulomb potential and was used in this work, greatly improves the description of band structures, including band gaps. The cut-off energy in the plane wave expansion was set to 500 eV. Atomic positions were relaxed until the forces on the atoms were smaller than 0.01 eV/Å. For Brillouin zone integration, we used the Monkhorst-Pack *k*-mesh

scheme with 7×13×13 when calculating the total energy and band structure. A supercell (1×5×5, P*nma*) with 200 atoms was built containing one Sn atom replaced by Na/K for $Sn_{0.99}(Na,K)_{0.01}Se$. Another super cell (2×5×5, P*nma*) with 400 atoms was built for the Na/K dual-doped sample $Na_{0.005}K_{0.005}Sn_{0.99}Se$, which was relaxed with respect to both unit cell parameters and atomic positions before band structure calculations. In order to calculate defect formation energies for $Sn_{0.99}Na_{0.005}K_{0.005}Se$, the total energy of the supercell (1×5×5, Pnma) with 200 atoms, containing one Sn atom replaced by K, was also calculated. The charge carrier effective masses for the SnSe, $Sn_{0.99}(Na,K)_{0.01}Se$ and $Sn_{0.99}Na_{0.005}K_{0.005}Se$ were obtained from the band structure by taking a second derivative.

Table S2 SnSe and ASe (A = Na, K) formation energies, chemical potential differences between A and Sn, 'raw' Na, K and Na + K defect formation energies, and Na, K and Na + K defect formation energies calculated for the systems SnSe-ASe with A = Na, K

	SnSe	NaSe	KSe	Na 1%	K 1%	Na0.5%+K0.5%
ΔE_F^{SnSe} (eV/atom)	-0.483	-	-	-		-
ΔE_F^{NaSe} (eV/atom)	-	-0.571	-	-		-
ΔE_F^{KSe} (eV/atom)	-	-	-0.689	-		-
$\Delta\mu_{Na}$-$\Delta\mu_{Sn}$ (eV/2 atoms)	-	-	-	-0.176	-	-
$\Delta\mu_{K}$-$\Delta\mu_{Sn}$ (eV/2 atoms)	-	-	-	-	-0.412	-
$\Delta E_{F,\,raw}^{def}$ (eV/defect)	**-**	**-**	**-**	**-0.285**	**-0.196**	**-0.241**
ΔE_F^{def} (eV/defect)	**-**	**-**	**-**	**-0.109**	**0.216**	**0.053**

IV. Calculations of lattice thermal conductivity

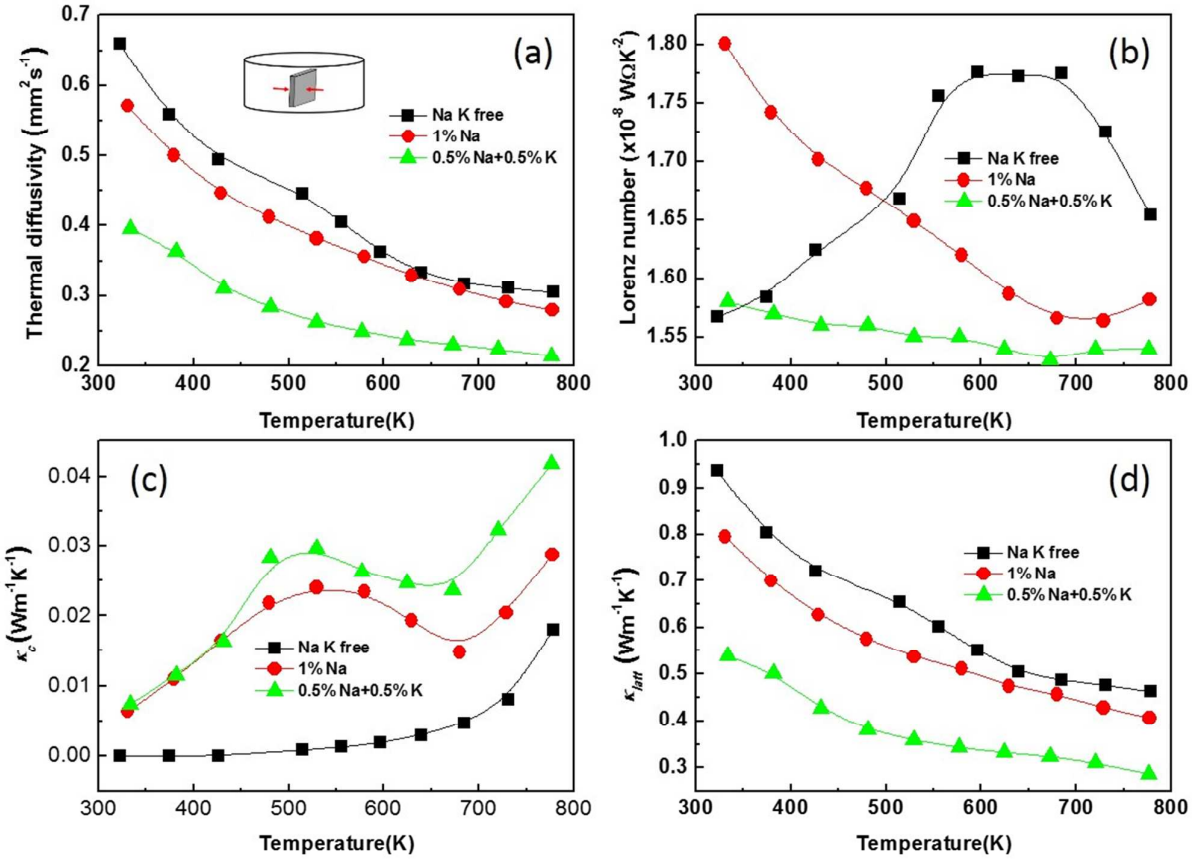

Figure S4 Temperature dependence of (a) thermal diffusivity, (b) Lorenz number, (c) carrier thermal conductivity and (d) lattice thermal conductivity for undoped, 1% Na-doped, and (0.5%Na + 0.5%K) co-doped SnSe.

The reduced Fermi energy was used to calculate the Lorenz number (Eq. 1), which varies as the Seebeck value changes (Eq. 2) with temperature or composition. The L calculation was estimated in a single parabolic band model (resulting in a value of L with a deviation of less than 10% when compared with a more rigorous single non-parabolic band and multiple band model calculation), as described in Ref. 8, 9, where the reduced Fermi energy was implicitly determined from the Seebeck values (Eq. 2).

$$L = \left(\frac{k_B}{e}\right)^2 \left(\frac{(r+7/2)F_{r+5/2}(\eta)}{(r+3/2)F_{r+1/2}(\eta)} - \left[\frac{(r+5/2)F_{r+3/2}(\eta)}{(r+3/2)F_{r+1/2}(\eta)}\right]^2 \right), \quad (1)$$

$$S = \pm \frac{k_B}{e}\left[\frac{(r+5/2)F_{r+3/2}(\eta)}{(r+3/2)F_{r+1/2}(\eta)} - \eta\right], \quad (2)$$

V. Calculation of lattice thermal conductivity based on Callaway's model

In order to understand the intrinsic relationship between the lattice thermal conductivities and precipitate size distributions and point defects, we performed a modified theoretical lattice thermal calculation based on Callaway's model[6], which depends primarily on the integration of the relaxation time scattered by Umklapp processes, phonon-phonon scattering, precipitates and point defects. In this work, grain boundary scattering was not taken into consideration, as the sizes of grain boundaries (hundreds of nm and even μm) are much larger than the mean free path for phonons in SnSe (several nm)[7,8]. The lattice thermal conductivity can be expressed in the form:

$$\kappa_{lat} = \frac{k_B}{2\pi^2\vartheta}\left(\frac{k_B T}{\hbar}\right)^3 \int_0^{\theta_D/T} \tau_c \frac{x^4 e^x}{(e^x-1)^2} dx \ , \quad (3)$$

where k_B is the Boltzmann constant, $\hbar$ is the reduced Planck constant, ϑ is the average sound (phonon-group) velocity, θ_D is the Debye temperature and x is defined as $\hbar\omega/k_B T$, and the total relaxation time calculated by the above scattering mechanisms is:

$$\tau_c^{-1} = \tau_U^{-1} + \tau_N^{-1} + \tau_P^{-1} + \tau_{PD}^{-1} \ . \quad (4)$$

The detailed expression for each item can be found elsewhere[9]. The contribution from precipitates can be described by a Mathiessen-type interpolation between the short- and long-wavelength scattering regimes[10,11], according to the expressions:

$$\tau_P^{-1} = \vartheta(\sigma_s^{-1} + \sigma_l^{-1})^{-1} V_P \quad (5)$$

$$\sigma_s = 2\pi R^2 \quad (6)$$

$$\sigma_l = \pi R^2 (\frac{\Delta D}{D})^2 (\frac{\omega R}{\vartheta})^4 \quad , \tag{7}$$

where D is the mass density, ΔD is the differrence in mass density between the nanoscale precipitate and the matrix and V_P is the density of the nanoscale precipitates. The contribution from point defects is given by the expressions[12]:

$$\tau_{PD}^{-1} = \frac{\omega^4 V_0}{4\pi\vartheta^3} \Gamma \tag{8}$$

$$\Gamma = \Gamma_M + \Gamma_S \tag{9}$$

$$\Gamma_M = \frac{\sum_{i=1}^{n} c_i (\frac{<M_i>}{M^*})^2 f_i^1 f_i^2 (\frac{M_i^1 - M_i^2}{<M_i>})^2}{\sum_{i=1}^{n} c_i} \tag{10}$$

$$\Gamma_S = \frac{\sum_{i=1}^{n} c_i (\frac{<M_i>}{M^*})^2 f_i^1 f_i^2 \varepsilon (\frac{r_i^1 - r_i^2}{<r_i>})^2}{\sum_{i=1}^{n} c_i} \quad , \tag{11}$$

where V_0 is the volume per atom, Γ is the disorder scaling parameter, which depends on mass, Γ_M, and strain, Γ_S, field fluctuations, c_i is the degeneracy (here $c_1 = c_2 = 1$), f_i is the fractional occupation, $< r_i >$ is the average radius, $< M_i >$ is the average mass of each sub-lattice, M^* is the average atomic mass of the compound, and ε is a function of the Gruneisen parameter, which characterizes the anharmonicity of the lattice.

In combination with TEM observations to obtain the required structural parameters, including the radius and the number density of precipitates, the lattice thermal conductivities could be calculated for each chemical composition in the differently doped samples. The parameters that were used in the lattice thermal conductivity calculation are listed in **Tables S3** and **S4**.

Table S3 Parameters for lattice thermal conductivity calculations

Parameter	Symbol	Unit	SnSe
Density of mass	D	g/cm^3	6180
Density of Precipitate	D	g/cm^3	2620 (Na_2Se)
			2290 (K_2Se)
Debye Temperature	θ_D	K	142[8]
Sound velocity	ϑ	m/s	1674[13]
Gruneisen parameter	γ		3.13[8]
Volume per atom	V_0	/angstrom^3	212.39
	ε		135[7]
Ratio of normal to Umklapp	β		0.85 (fitted)

Table S4 Atomic information for point defects

Atomic Mass/amu	**M_{Sn}**	**118.71**
	M_{Se}	78.96
	M_{Na}	22.99
	M_K	39.098
Radius/pm	r_{Sn}	145
	r_{Se}	103
	r_{Na}	190
	r_K	243

VI. Carrier concentration and carrier mobility

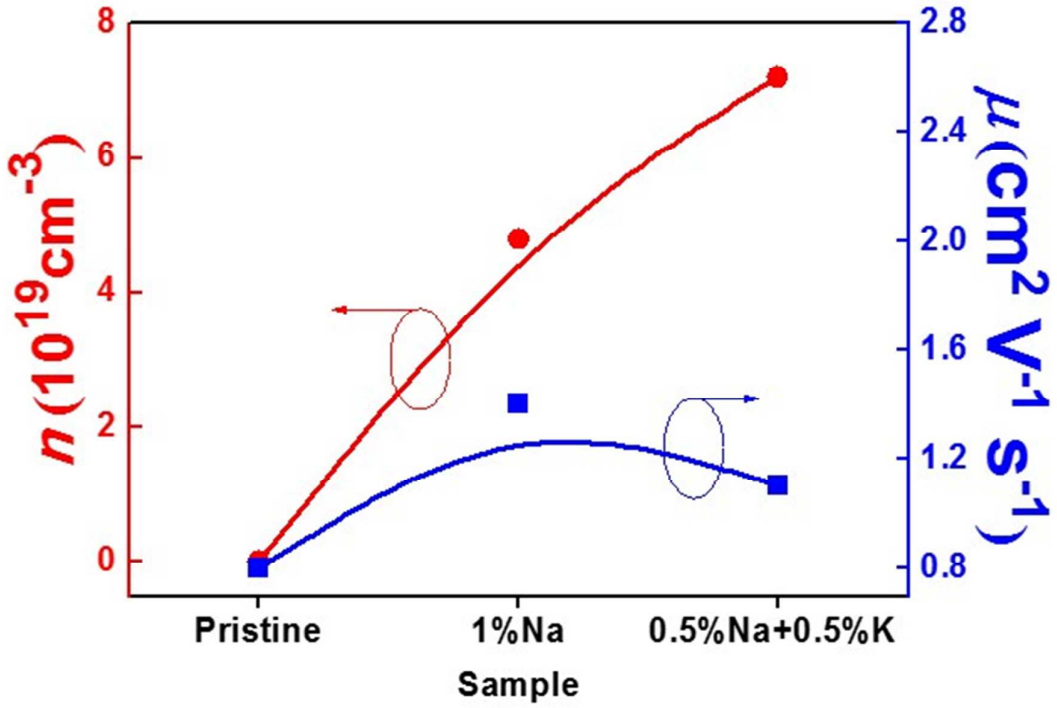

Figure S5 Carrier concentration and carrier mobility for the three bulk samples.

References

(1) Kovács, A.; Schierholz, R.; Tillmann, K. *J. Large-Scale Res. Facil. JLSRF* **2016**, *2*.
(2) Hohenberg, P.; Kohn, W. *Phys. Rev.* **1964**, *136*, B864.
(3) M D Segall and Philip J D Lindan and M J Probert and C J Pickard and P J Hasnip and S J Clark and M C Payne. *J. Phys. Condens. Matter* **2002**, *14*, 2717.
(4) Kohn, W.; Sham, L. J. *Phys. Rev.* **1965**, *140*, A1133.
(5) Heyd, J.; Scuseria, G. E.; Ernzerhof, M. *J. Chem. Phys.* **2003**, *118*, 8207.
(6) Callaway, J. *Phys. Rev.* **1959**, *113*, 1046.
(7) Wei, T.-R.; Wu, C.-F.; Zhang, X.; Tan, Q.; Sun, L.; Pan, Y.; Li, J.-F. *Phys Chem Chem Phys* **2015**, *17*, 30102.
(8) Xiao, Y.; Chang, C.; Pei, Y.; Wu, D.; Peng, K.; Zhou, X.; Gong, S.; He, J.; Zhang, Y.; Zeng, Z.; Zhao, L.-D. *Phys. Rev. B* **2016**, *94*.125230.
(9) Lo, S.-H.; He, J.; Biswas, K.; Kanatzidis, M. G.; Dravid, V. P. *Adv. Funct. Mater.* **2012**, *22*, 5175.
(10) Kim, W.; Majumdar, A. *J. Appl. Phys.* **2006**, *99*, 084306.
(11) Mingo, N.; Hauser, D.; Kobayashi, N. P.; Plissonnier, M.; Shakouri, A. *Nano Lett.* **2009**, *9*, 711.
(12) Yang, J.; Meisner, G. P. *Appl. Phys. Lett.* **2004**, *85*, 1140.
(13) Zhao, L.-D.; Lo, S.-H.; Zhang, Y.; Sun, H.; Tan, G.; Uher, C.; Wolverton, C.; Dravid, V. P.; Kanatzidis, M. G. *Nature* **2014**, *508*, 373.